Geochemistry Geophysics Geosystems G3
AN ELECTRONIC JOURNAL OF THE EARTH SCIENCES
Published by AGU and the Geochemical Society

Article
Volume 4, Number 9
9 September 2003
1073, doi:10.1029/2002GC000433
ISSN: 1525-2027

A new parameterization of hydrous mantle melting

Richard F. Katz and Marc Spiegelman
Lamont-Doherty Earth Observatory of Columbia University, Palisades, New York 10964, USA (katz@ldeo.columbia.edu)

Charles H. Langmuir
Department of Earth and Planetary Sciences, Harvard University, Cambridge, Massachusetts 02138, USA

[1] Modeling of melt formation and transport in all tectonic settings requires the inclusion of water, since water has large effects on mantle solidi as well as physical properties of liquids. To facilitate the inclusion of water in melting models this paper presents a new parameterization for melt fraction as a function of pressure, temperature, water content and modal cpx, based on knowledge gained from recent advances in the fields of thermodynamic modeling as well as experimental investigations of peridotite melting and hydrous equilibria. The parameterization is computationally efficient and can be modified easily as better experimental data become available. We compare it to other published parameterizations and test it in simple calculations of adiabatic decompression melting (mid-ocean ridge) and hydrous melting (subduction zone).

Components: 8542 words, 12 figures, 3 tables.

Keywords: Mantle; hydrous; melt; parameterization; cpx; peridotite.

Index Terms: 3640 Mineralogy and Petrology: Igneous petrology; 3210 Mathematical Geophysics: Modeling; 3230 Mathematical Geophysics: Numerical solutions.

Received 29 August 2002; **Revised** 22 May 2003; **Accepted** 28 May 2003; **Published** 9 September 2003.

Katz, R. F., M. Spiegelman, and C. H. Langmuir, A new parameterization of hydrous mantle melting, *Geochem. Geophys. Geosyst.*, *4*(9), 1073, doi:10.1029/2002GC000433, 2003.

1. Introduction

[2] Magma genesis and transport in subduction zones influence large scale chemical cycling in the mantle and provide the crucial link between mantle dynamics and geochemical signals observed in island arcs. Nevertheless, many aspects of these processes are still poorly understood. The challenge remains to integrate theory, experiment and observation into a consistent framework that permits inferences on subduction zone chemistry and dynamics from available observations. Quantitative models of subduction zones provide such a framework. To consistently model both solid and fluid/melt processes, however, requires an accurate and computationally efficient parameterization of mantle melting that includes the effects of significant amounts of water. We present here a new parameterization that, while remaining mathematically simple, succeeds in capturing the important features of the behavior of this complex thermodynamic system.

[3] While a full thermodynamically consistent treatment of melting might be preferred, current equilibrium thermodynamic models such as MELTS and pMELTS [*Ghiorso*, 1994; *Ghiorso and Sack*, 1995; *Ghiorso et al.*, 2002; *Asimow*

and Stolper, 1999] remain too computationally expensive for large time-dependent 2-D calculations (although see *Tirone and Ganguly* [2002]) that are necessary to create quantitative models applicable to ridges and convergent margins. Furthermore, these models do not cover the full range of pressure, temperature and composition conditions relevant to subduction zones. Thus melting parameterizations are a useful way to incorporate melting into tectonic models and these parameterizations also have the advantage that they often better reproduce existing experimental data.

[4] Thermodynamic constraints on such models, however, are also important. As we show, current experimental data for wet melting is sparse and experimental data for dry melting shows a large amount of scatter, even on nominally identical samples (see also *Hirschmann* [2000]). In order to make progress, here we take an approach that incorporates many of the theoretical concepts from thermodynamic models and also calibrates them against the current experimental database.

[5] Other workers have produced various parameterizations [*McKenzie and Bickle*, 1988; *Davies and Bickle*, 1991; *Langmuir et al.*, 1992; *Kinzler and Grove*, 1992; *Jha et al.*, 1994; *Iwamori et al.*, 1995; *Iwamori*, 1997; *Kinzler*, 1997]; the discussion below presents a comparison of the different models. Overall, many of the parameterizations are qualitatively similar to each other with different biases in different parts of parameter space. Further progress in refining parametric melting functions will require either additional experiments or concerted efforts to better quantify the uncertainty in the experimental database.

1.1. Basic Structure of the Parameterization

[6] Our parameterization is of the form $F = f(P, T, X_{H_2O}, M_{cpx})$ where F is the weight fraction of melt present, P is the pressure in GPa, T is the temperature in degrees Celsius, X_{H_2O} is weight fraction of water dissolved in the melt and M_{cpx} is the modal cpx of the unmelted (or residual) peridotite. This parameterization incorporates the following concepts and principles:

[7] 1. The isobaric melting function, F should be monotonically increasing, concave upward, with isobaric productivity, $\partial F/\partial T|_{P,X_{H_2O}}$ increasing as a function of T [*Hirschmann et al.*, 1999], as long as the phase assemblage remains constant. We utilize this constraint despite the fact that existing experimental data do not clearly show the effect.

[8] 2. $F(T)$ should be kinked when major phases are exhausted from the residue, such as when $F = F_{cpx-out}$. In other words, productivity should decrease discontinuously at this point and then rise as it did for melting in the low-F regime [*Hirschmann et al.*, 1999].

[9] 3. For a peridotite with fertile mineral compositions, the melt reaction coefficient of cpx is a function of pressure only. Thus $F_{cpx-out}$ can be predicted given the modal cpx of the peridotite being melted and the pressure of melting. [*Pickering-Witter and Johnston*, 2000; *Longhi*, 2002; *Walter*, 1998; *Walter et al.*, 1995].

[10] 4. Addition of water to a peridotite system should monotonically increase F at constant T and P. $F(X_{H_2O})$ at constant temperature and pressure should be an approximately linear increasing function for small $X^{bulk}_{H_2O}$. Furthermore, the slope should increase with increasing temperature, [*Hirschmann et al.*, 1999; *Hirose and Kawamoto*, 1995; *Hirose*, 1997; *Gaetani and Grove*, 1998].

$$\left.\frac{\partial F}{\partial X^{bulk}_{H_2O}}\right|_{P,T} = c(T),\ c > 0. \tag{1}$$

[11] 5. Addition of water to a peridotite system should lower the solidus (except at atmospheric pressure) in proportion to X_{H_2O}. This seems to be uniform with P [*Burnham*, 1979]. It should also lower the liquidus of the solid. However, for melt fractions near one and modest bulk water content, the weight percent dissolved water at the liquidus is small because it is diluted by silicate melt. Thus the liquidus is not lowered substantially, except by extreme water contents.

[12] 6. Assuming, after *Michael* [1995] and *Asimow and Langmuir* [2003], that water may be treated as an incompatible element, addition of water to the system depresses the solidus until the melt becomes

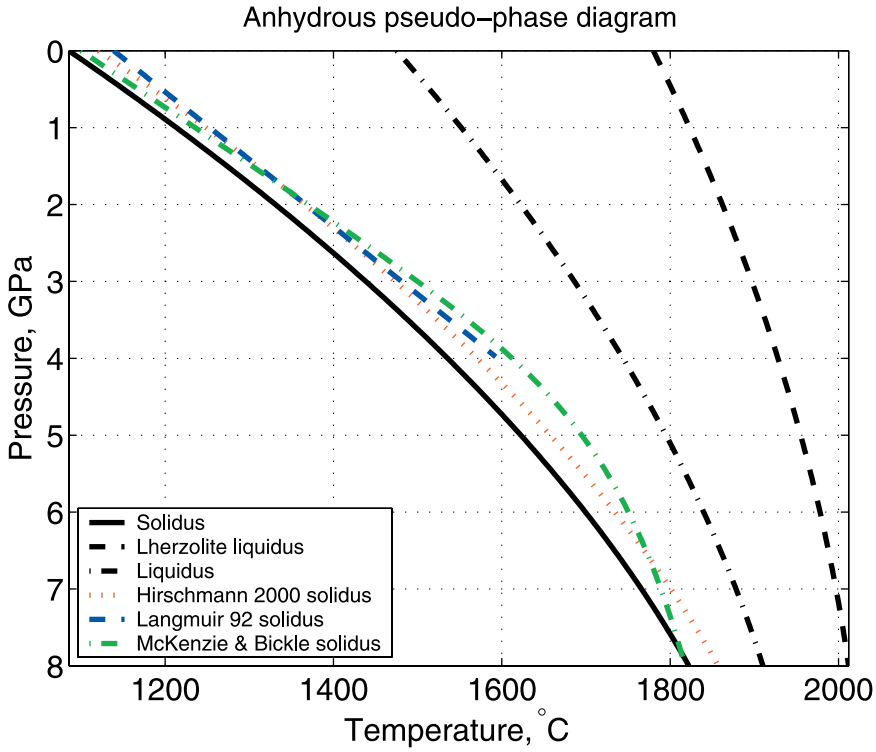

Figure 1. The anhydrous solidus, lherzolite liquidus (see text) and liquidus. Also shown, for comparison, the anhydrous solidi of *Hirschmann* [2000], *Langmuir et al.* [1992], and *McKenzie and Bickle* [1988].

saturated. Of course the amount of water at saturation is strongly dependent on pressure. Because the amount of water in the liquid decreases progressively as melting proceeds, the influence of water progressively decreases, and hence productivity above the wet solidus remains low until a temperature near the dry solidus is reached [*Hirth and Kohlstedt*, 1996; *Hirschmann et al.*, 1999].

[13] 7. Experiments show that $X_{H_2O}^{saturated}$ is zero at atmospheric pressure, about 13 wt% at 1 GPa and continues to rise with increasing pressure [*Dixon et al.*, 1995; *Mysen and Wheeler*, 2000].

2. Mathematical Formulation

2.1. Anhydrous Melting

[14] F_{cpx} is the degree of melting expected by equilibrium batch melting prior to the exhaustion of cpx. We parameterize it as a power-law of the rescaled temperature T'.

$$F_{cpx}(T') = [T'(T,P)]^{\beta_1}, \tag{2}$$

where

$$T'(T,P) = \frac{T - T_{solidus}(P)}{T_{liquidus}^{lherz}(P) - T_{solidus}(P)}. \tag{3}$$

is the fractional distance in temperature between the solidus and "lherzolite liquidus" (defined below). Here T is the temperature in Kelvin and the pressure dependence is hidden in $T_{solidus}$ and $T_{liquidus}^{lherz}$. Using the form suggested by *Hirschmann* [2000],

$$T_{solidus} = A_1 + A_2 P + A_3 P^2, \tag{4}$$

$$T_{liquidus}^{lherz} = B_1 + B_2 P + B_3 P^2, \tag{5}$$

for pressure in GPa (Figure 1). The "lherzolite liquidus," $T_{liquidus}^{lherz}$, in equation (2) is introduced as a means for creating a kinked melting function. It can be conceptualized as the temperature that the liquidus would have if melting continued according to equation (2) to $F = 1$, i.e., with cpx remaining in the residue. Cpx-out occurs at some $F < 1$, and at this point there is a discontinuous

change in the productivity of the system. For simplicity, we do not consider the effect on melt productivity of the exhaustion of the aluminous phase, although *Walter* [1998] has shown that the exhaustion of garnet occurs before the exhaustion of cpx at pressures between 2 and 4 GPa. Furthermore, we ignore the loss of opx from the residue as this typically occurs at melt fractions beyond what we expect in an arc setting (thus we do not define a "hartzburgite liquidus"). For a closed (batch) system,

$$F_{cpx-out} = \frac{M_{cpx}}{R_{cpx}(P)}. \tag{6}$$

M_{cpx} is the weight fraction of cpx in the solid peridotite being isobarically melted. R_{cpx} is the reaction coefficient for cpx in the melting reaction. Following experimental results of *Longhi* [2002], *Walter* [1998], *Walter et al.* [1995] and *Pickering-Witter and Johnston* [2000], we give this reaction coefficient a pressure dependence of the form

$$R_{cpx}(P) = r_0 + r_1 P. \tag{7}$$

There is evidence from *Walter* [1998] and *Kelemen et al.* [1992] that R_{cpx} reaches a maximum at about 3.5 GPa and decreases at higher pressures (in the garnet stability field). For simplicity, we neglect this effect but it may need to be reconsidered for applications where significant melting occurs at pressures greater than 3.5 GPa.

[15] For $F > F_{cpx-out}$, the melting reaction changes to consume mostly opx and the melting function is:

$$F_{opx}(T) = F_{cpx-out} + \left(1 - F_{cpx-out}\right)\left[\frac{T - T_{cpx-out}}{T_{liquidus} - T_{cpx-out}}\right]^{\beta_2}, \tag{8}$$

where

$$T_{cpx-out} = F_{cpx-out}^{\frac{1}{\beta_1}}\left(T_{liquidus}^{lherz} - T_{solidus}\right) + T_{solidus} \tag{9}$$

and $T_{liquidus}$ is the true liquidus of the model peridotite system (Figure 1),

$$T_{liquidus} = C_1 + C_2 P + C_3 P^2. \tag{10}$$

The shape of the overall melting function at different pressures is shown in Figure 2. As mentioned in the introduction, $\partial^2 F/\partial^2 T|_{P, X_{H2}O} > 0$ for the isobaric melting curves and they are kinked at cpx out. The pressure dependence of R_{cpx} is evident in the melt fraction at which cpx is exhausted from the residue.

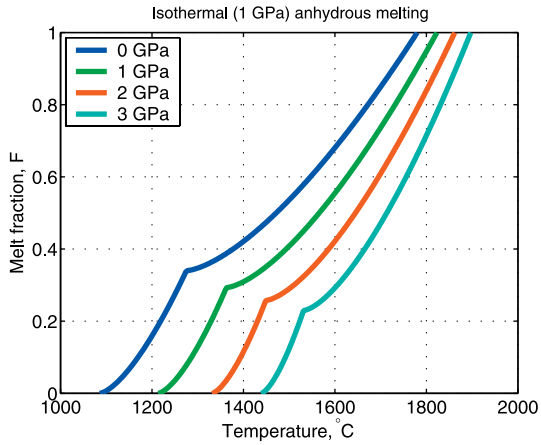

Figure 2. Isobaric anhydrous melting curves at different pressures with modal cpx of the unmelted rock at 15 wt%. For a comparison of these calculations to data, see Figure 6.

2.2. Hydrous Melting Extension

[16] This parameterization of dry melting can be extended to include systems where the dissolved water fraction in the melt in weight fraction, X_{H_2O}, is specified (the weight fraction of bulk water is written as $X_{H_2O}^{bulk}$). Specifically, the changes are the following:

$$T_{solidus}(P) \rightarrow T_{solidus}(P) - \Delta T(X_{\mathrm{H_2O}}) \tag{11}$$

$$T_{liquidus}^{lherz}(P) \rightarrow T_{liquidus}^{lherz}(P) - \Delta T(X_{\mathrm{H_2O}}) \tag{12}$$

$$T_{liquidus}(P) \rightarrow T_{liquidus}(P) - \Delta T(X_{\mathrm{H_2O}}) \tag{13}$$

where $\Delta T(X_{\mathrm{H_2O}})$ is the temperature decrease in the solidus caused by a water content $X_{\mathrm{H_2O}}$ in the melt. This function, the same for the liquidus, lherzolite liquidus and solidus, may take a variety of forms as long as they satisfy:

$$\Delta T(X_{\mathrm{H_2O}} = 0) = 0, \tag{14}$$

$$\Delta T\left(X_{\mathrm{H_2O}} \geq X_{\mathrm{H_2O}}^{sat}\right) = \Delta T\left(X_{\mathrm{H_2O}}^{sat}\right). \tag{15}$$

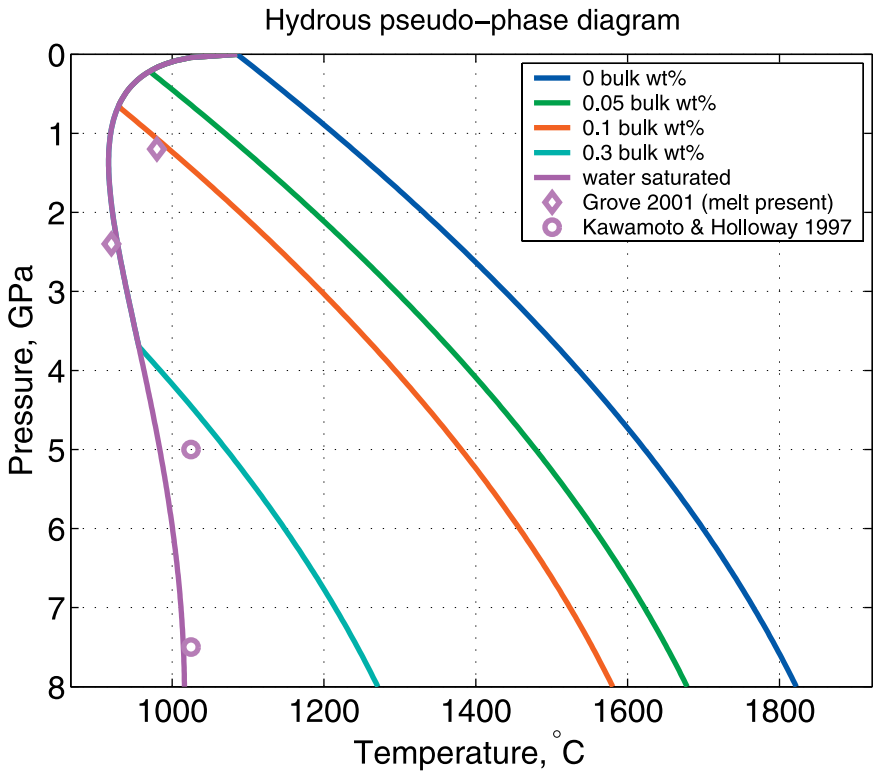

Figure 3. The solidus for different bulk water contents of the system. Solidus depression is linear with dissolved water. It is bounded by the saturation of water in the melt, a function of pressure.

where $X^{sat}_{H_2O}(P)$ is the weight percent of water in a completely saturated melt, which is principally a function of pressure. The criterion stated in equation (15) is necessary because of the way that we handle a free vapor phase. For computational simplicity, water present beyond the saturation of the melt is not computed as a separate vapor phase, it is accounted for as a part of the fluid phase which also includes the saturated silicate melt. The thermodynamic properties (e.g., liquidus) of the silicate melt are unaffected by water content beyond saturation. The utility of this simplification is that it permits the use of a standard two-phase fluid mechanical formulation for melt transport [*McKenzie*, 1984; *Spiegelman*, 1993].

[17] The speciation of water dissolved in silicate melt has been a subject of debate (for a summary and references [see *Withers et al.*, 1999]). *Stolper* [1989] and *Ihinger et al.* [1999] have reported that at temperatures near the water saturated rhyolite solidus, the first 1–2 wt% water dissolved into the melt exists mostly as hydroxyl ions (although see *Mosenfelder et al.* [2002]). For higher dissolved water contents, molecular water becomes the dominant species, however, increasing temperature diminishes the proportion of molecular water. The depolymerizing effect of hydroxyl ions on silicate melt exceeds that of molecular water because of its non-zero charge; depolymerization of the melt increases its entropy, stabilizing it at lower temperatures. Thus we choose a form for $\Delta T(X_{H_2O})$ that has a steep slope at low water contents and grows more slowly after that. This form is consistent with the data shown in Figure 8a, within their uncertainties.

$$\Delta T(X_{H_2O}) = K X^{\gamma}_{H_2O}, \quad 0 < \gamma < 1 \tag{16}$$

The calibration of this function to find K and γ is discussed below. Figure 3 shows the solidus for a range of bulk water contents.

[18] The saturation concentration of water in the melt is constrained at pressure below 2 GPa by the experiments of *Dixon et al.* [1995] and *Mysen and*

Wheeler [2000]. At higher pressure we estimate the saturation concentration of water by requiring that, in conjunction with $\Delta T(X^{sat}_{H_2O})$, it be consistent with the the results of *Grove* [2001] and *Kawamoto and Holloway* [1997] on the water saturated solidus.

$$X^{sat}_{H_2O} = \chi_1 P^{\lambda} + \chi_2 P, \quad 0 < \lambda < 1. \tag{17}$$

Calibration of this equation is discussed below.

[19] The systematics of water abundances in MORB demonstrate that water behaves similarly to other moderately incompatible elements. *Michael* [1995] has shown that the water/Ce ratio changes little in MORB, and hence that water has approximately the same D as Ce for the melting conditions beneath ocean ridges. This behavior can be understood with the recognition that water is incorporated in solid mantle phases, like other trace components. Many workers have assumed that there is always a vapor phase at the solidus of materials that contain water (T. Grove, personal communication); however, the treatment of water as a trace element in solution in solid phases suggests that this is not the case. Requiring water saturation at the solidus is similar to insisting on saturation of some rare earth element phase at the solidus. That only takes place if the concentration of the component exceeds the amount that can be taken into solution by the solid phases. Furthermore, partition coefficients can be used successfully even for major constituents of phases, and this use is thermodynamically valid [*Langmuir and Hanson*, 1981; *Weaver and Langmuir*, 1990]. By considering water to behave as a regular trace element, its equilibrium partitioning between solid and silicate melt can be modeled with a bulk distribution coefficient:

$$X_{H_2O} = \frac{X^{bulk}_{H_2O}}{D_{H_2O} + F(1 - D_{H_2O})}. \tag{18}$$

The parameterization described here does not preclude the use of a bulk D_{H_2O} for water that varies with pressure. While such a variation is expected in natural systems and has been considered in past work by *Hirth and Kohlstedt* [1996], a quantitative estimate of $D_{H_2O}(P)$ for the range of water content and pressure relevant to arc melting has not been produced. Thus in order to preserve the simplicity and transparency of the melting parameterization, we choose a constant bulk partitioning coefficient for the calculations described here. On the basis of its similarity in behavior to Ce, we use a D for water of 0.01. However, we do so with the recognition that this choice will have important implications for the volume and chemistry of melt produced near the wet solidus in arc melting simulations. Possible effects of variation in D_{H_2O} need to be considered in the detailed application of the model.

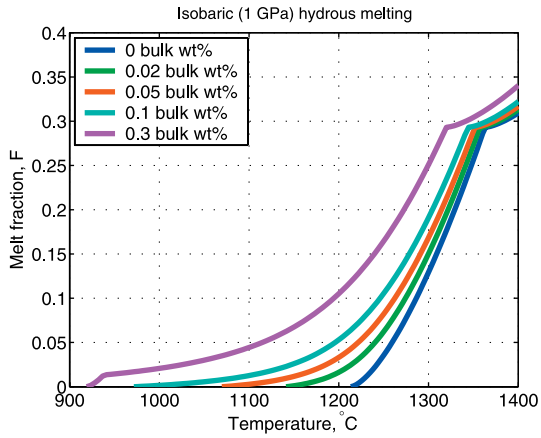

Figure 4. Isobaric melting curves (for 1 GPa) with different bulk water contents. The 0.3 wt% melting curve is saturated at the solidus.

[20] Because ΔT depends on the melt fraction, F appears on both sides of equation (19) and no closed form analytical solution for F exists; however, a solution can be found numerically using a root-finder. The total melting function for $F \leq F_{cpx-out}$ is

$$F\left(P, T, X^{bulk}_{H_2O}\right) = \left[\frac{T - \left(T_{solidus} - \Delta T\left(X_{H_2O}\left(X^{bulk}_{H_2O}, P, F\right)\right)\right)}{T^{lherz}_{liquidus} - T_{solidus}}\right]^{\beta_1}. \tag{19}$$

[21] Figure 4 shows isobaric melting curves with different bulk water content. Notice that small additions of water greatly depress the solidus and produce a prominent "low-F tail" without generating much additional melt. However, with water contents exceeding saturation at the solidus (0.3 wt% bulk water in Figure 4), the melting function takes on a qualitatively different shape,

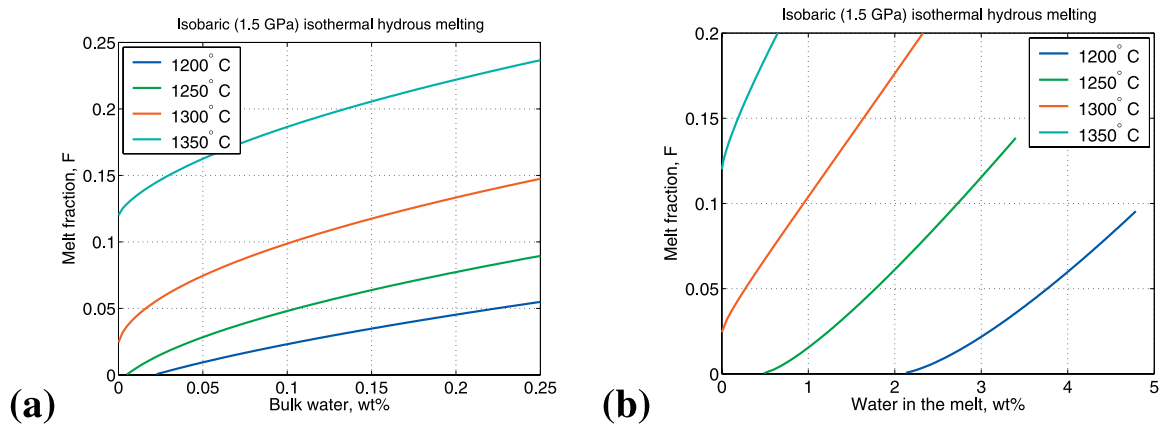

Figure 5. Degree of melting as a function of the water in the system, holding the temperature (see figure) and pressure (1.5 GPa) constant. Modal cpx is 17% in the unmelted solid. (a) F as a function of $X_{H_2O}^{bulk}$. Compare to *Gaetani and Grove* [1998, Figure 13a]. (b) F as a function of water dissolved in the melt. Bulk distribution coefficient of water is assumed to be 0.01.

ramping up sharply in F just above the solidus. This represents eutectic-like melting due to the overabundance of water acting as an additional phase: with each increment of new melting, more water can dissolve into the melt, pinning the solidus at its water saturated temperature until the reservoir of vapor phase water has been exhausted [*Gaetani and Grove*, 1998]. At pressures below 2 GPa, water partitioning at the solidus is strongly affected by the presence of amphibole [*Schmidt and Poli*, 1998]. A more sophisticated parameterization should take this into account.

[22] Figures 5a and 5b show isobaric, isothermal melting curves. Progressive melting is achieved by adding water to the system. At $X_{H_2O}^{bulk}$ below saturation of the melt, most of the water goes into the melt, lowering the solidus and increasing the degree of melting. Figure 5a shows F as a function of bulk water content. This figure demonstrates that our parameterization achieves the objective stated in the introduction in item 4: the isobaric isothermal melting function has a roughly linear dependence on bulk water content, with a slope that is larger for higher temperature.

[23] The equations described above provide a quantitative framework for equilibrium melting of peridotite in the presence of water. To make this framework useful we must specify values of the model parameters A_n, B_n, C_n, r_n, K, γ, χ_n, λ and β_n. This is done using a database of experimental results from the literature and comparison to other established models.

3. Experimental Database

3.1. Anhydrous

[24] Calibration of the anhydrous model was performed on a set of experimental results on peridotite melting from various authors and labs. These results were compiled from publications from 1980 to the present. The peridotites used in melting experiments in the experimental database are compiled in Table 1. Some of these studies contain results than are not included in the database due to undetermined or zero melt fraction.

[25] A sampling bias of experiments especially relevant to this study is the lack of data at low melt fractions. Determining the compositions of melts at low melt fraction (below about 2 wt%) is difficult and unreliable and thus mass-balance estimates of F in this range can be inaccurate. However, understanding the beginning of melting is crucial because low-F melts control much of the trace element budget. The treatment of this problem is discussed in greater detail in the next section.

[26] While typically reported experimental errors in P, T, and F are approximately 1 kb, 5°C and 1 wt% respectively, a glance at plots of the database reveal that there is significant variability between different experiments at different labs under nominally the

Table 1. Summary of Experimental Peridotites (Anhydrous Experiments Only)

Identifier	Rock Type	Modal cpx, %	Authors
KLB-1	Spinel Lherzolite	15	*Hirose and Kushiro* [1993] *Iwamori et al.* [1995] *Takahashi et al.* [1993] *Takahashi* [1986]
HK66	Spinel Lherzolite	14	*Hirose and Kushiro* [1993]
KR4003	Spinel Lherzolite	15	*Walter* [1998]
MM3	Synthetic Spinel Lherzolite[b]	17	*Baker and Stolper* [1994] *Baker et al.* [1995] *Falloon et al.* [1999]
FER-B	Synthetic Spinel Lherzolite[b]	40	*Pickering-Witter and Johnston* [2000]
FER-C	Synthetic Spinel Lherzolite[b]	1	*Pickering-Witter and Johnston* [2000]
FER-D	Synthetic Spinel Lherzolite[b]	10	*Pickering-Witter and Johnston* [2000]
FER-E	Synthetic Spinel Lherzolite[b]	23.5	*Pickering-Witter and Johnston* [2000]
PHN1661	Garnet Lherzolite	16[a]	*Kushiro* [1996]
KG1	Spinel Lherzolite + Basalt	16[a]	*Kogiso et al.* [1998]
KG2	Spinel Lherzolite + Basalt	16[a]	*Kogiso et al.* [1998]
Hawaiian	Pyrolite	16[a]	*Jaques and Green* [1980]
Tinaquillo1	Spinel Lherzolite	16[a]	*Jaques and Green* [1980] *Robinson et al.* [1998]
Tinaquillo8	Spinel Lherzolite	16[a]	*Robinson et al.* [1998]

[a] Modal cpx not known or not available. The mean of the other peridotites, 16%, is assumed for computations here.
[b] Constructed by combining mineral separates from the Kilbourne Hole Xenolith.

same conditions (see Figure 6). For example, in Figure 6a, pressure is known exactly (1 atm) and composition is constant across experiments; yet experiments conducted at 1175, 1200 and 1250°C each show a spread of about 10 wt% in melt fraction. Uncertainty in pressure, especially above ~4 GPa, and in temperature may be underestimated by experimentalists (J. Longhi, personal communication). However, isothermal productivity only amounts to about −2 wt% per kilobar and so it is not able to explain all the variability. Hard to control experimental parameters such as oxygen fugacity, iron loss to the container, small amounts of water present in nominally anhydrous runs, run duration and physical properties of the starting materials probably all play a role in producing this disagreement. Until we have a better understanding of the formal error associated with experimental studies of melting, a partial reliance on theory and expectations is necessary.

3.2. Hydrous

[27] Experiments on hydrous melting of peridotite are few. Fortunately there exist several sets of experiments that can be used as a foundation to calibrate the model. One set, from *Hirose and Kawamoto* [1995] is a direct melting type experiment where samples of peridotite with known bulk water are melted and the degree of melting is determined using mass balance of sodium. (*Hirose and Kawamoto* [1995] assumed that sodium is completely incompatible when calculating the melt fraction. We recalculated the degree of melting after *Hirschmann* [2000] based on the assumption that Na has a small but non-zero partition coefficient when cpx is present.) The second, by *Gaetani and Grove* [1998], is a set of peridotite melting experiments that do not attempt to measure an equilibrium degree of melting of a peridotite. Instead they use the fact that the degree of melting is an extensive property and maximize the yield of melt by varying the bulk composition, giving a large enough proportion of glass after quench to accurately determine the composition of the glass [see also *Kinzler and Grove*, 1992]. Although this does not give the needed information, $F(X_{H_2O})$ directly, it is an advantageous approach because it allows an accurate analytical determination of the amount of water dissolved in the melt that is not dependent on assumptions regarding water loss to the capsule or partitioning of trace elements.

4. Model Calibration

4.1. Anhydrous Melting

[28] Calibration of the anhydrous model requires assigning numerical values to the parameters A_n,

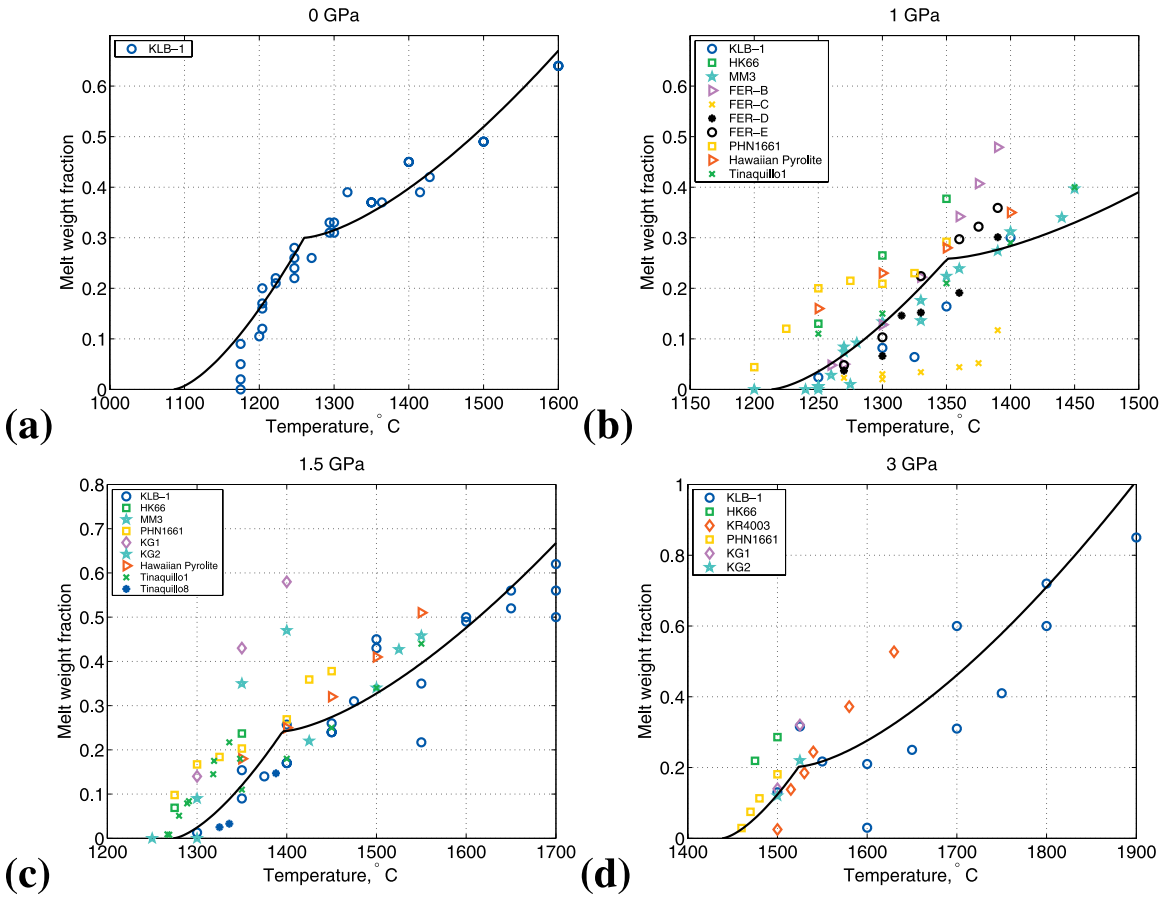

Figure 6. The melting model with modal cpx at 15 wt% compared to isobaric subsets from the experimental database. Note that experimental results represent a range of starting compositions in terms of modal mineralogy and mineral fertility. Commonly used KLB-1 has 15 wt% cpx. Note the variability among nominally comparable experiments in P, T and composition. (a) 0 GPa, (b) 1 GPa, (c) 1.5 GPa, and (d) 3 GPa.

B_n, C_n, r_n, and β_n that provide a "best fit" to the assemblage of data, theory and expectations available (see Table 2). This procedure is not an explicit inversion but occurs interactively by adjusting model parameters and comparing resulting curves to data and to expected trends such as productivity functions ($\partial F/\partial T|_{P,X_{H_2O}}$, $\partial F/\partial T|_{T,X_{H2}O}$, and $\partial F/\partial X_{H_2O}|_{P,T}$) and how they vary with changes in the main variables.

[29] The cpx reaction rate constants, r_0 and r_1, are constrained on the basis of experiments on a simplified chemical system at 1% melting by *Longhi* [2002] and by batch melting experiments of lherzolite by *Pickering-Witter and Johnston* [2000], *Walter et al.* [1995], and *Walter* [1998]. We fix values of r_n by informally fitting the anhydrous database.

[30] *Hirschmann* [2000] and *Schwab and Johnston* [2001] show that significant variability in the solidus temperature between different compositions is due, at least in part, to the fertility of the peridotite. *Hirschmann* [2000] chose a set of experiments that represent an intermediate composition and formally inverted these for a solidus of best fit. This fit was performed using a melt present/absent criterion and did not utilize information on melt fraction for experiments with melt present. Using our database of melt fraction and melting parameterization, we find that a constant shift in the *Hirschmann* [2000] solidus of 35° down in temperature lowers the RMS residual of the model fit and better matches the data above the solidus (see Figure 7). Because we expect a small "low-F tail" in the anhydrous isobaric melting function we assign a value of β_1 that is greater

Table 2. Summary of Parameters and Values

Parameter	For Calculating	Value	Units
A_1	$T_{solidus}$	1085.7	°C
A_2		132.9	°C GPa^{-1}
A_3		−5.1	°C GPa^{-2}
B_1	$T^{lherz}_{liquidus}$	1475.0	°C
B_2		80.0	°C GPa^{-1}
B_3		−3.2	°C GPa^{-2}
C_1	$T_{liquidus}$	1780.0	°C
C_2		45.0	°C GPa^{-1}
C_3		−2.0	°C GPa^{-2}
r_1	R_{cpx}	0.50	cpx/melt
r_2		0.08	cpx/melt/GPa
β_1	F	1.50	
β_2		1.50	
K	$\Delta T(X_{H_2O})$	43	°C wt%$^{-\gamma}$
γ		0.75	
D_{H_2O}		0.01	
χ_1	$X^{sat}_{H_2O}$	12.00	wt% GPa$^{-\lambda}$
χ_2		1.00	wt% GPa^{-1}
λ		0.60	
c_P	$\left.\frac{dF}{dP}\right\|_S$	1000	J kg^{-1} K^{-1}
α_s		40	$\times 10^{-6}$ K^{-1}
α_f		68	$\times 10^{-6}$ K^{-1}
ρ_s		3.30	$\times 10^{3}$ kg m^{-3}
ρ_f		2.90	$\times 10^{3}$ kg m^{-3}
ΔS		300	J kg^{-1} K^{-1}

than 1. The anhydrous liquidii ($T^{lherz}_{liquidus}(P)$ and $T_{liquidus}(P)$) are constrained mainly by fitting the melting function $F(T')$ to the anhydrous data set.

4.2. Hydrous Melting

[31] There are two components to the hydrous melting extension of our parameterization: the solidus shift as a function of water dissolved in the melt and the saturation water content of the silicate melt as a function of pressure.

[32] At low pressures, both $\Delta T(X_{H_2O})$ and $X^{sat}_{H_2O}(P)$ are constrained by data. Water solubility measurements by *Dixon et al.* [1995] and *Mysen and Wheeler* [2000] on different melt compositions (*Dixon et al.* [1995] uses basalt, [*Mysen and Wheeler*, 2000] uses haploandesite. The haploandesites have a higher silica content than the basalts.) are used to constrain the saturation water content of basaltic melt below two GPa.

[33] We calibrate $\Delta T(X_{H_2O})$ using an approach similar to that sketched by *Gaetani and Grove* [1998]. The calibration is performed using a model for magnesium partitioning between the residual olivine and the melt [*Langmuir et al.*, 1992; *Asimow*, 2000] that is able to give the liquidus temperature for the major element compositions of the experiments recalculated water free. Comparing this temperature to the water-bearing experiment gives the temperature change associated with the water content. *Gaetani and Grove* [1998] also give a calibration for dry olivine liquidus temperatures that they use for a similar purpose, but their form is essentially identical to that of *Langmuir et al.* [1992] and demonstrates the same compositional dependence. For this paper we calibrate the model based on a set of experimental melts encompassing a larger parameter space in P, T, and X_{H_2O} (P. Asimow, personal communication). The data generated using this inversion of chemistry are shown in Figure 8a.

[34] At pressures above two GPa we have no direct constraints on $X^{sat}_{H_2O}$. Instead we use an indirect constraint from measurements of the water saturated solidus by *Kawamoto and Holloway* [1997] and *Grove* [2001]. In these experiments, however, the water content of the saturated melt is not reported. By taking the parameterized dry solidus minus the experimentally determined water saturated solidus we can estimate the ΔT of the solidus for each experiment. To estimate the water content of these saturated melts we employ our parameterization of water solubility in the melt from equation (17) (which, unfortunately is not well constrained at high pressure). Data derived in this way, and the resulting fit for $\Delta T(X_{H_2O})$, is shown in Figure 8a. As explained above, this does not limit the concentration of water in the fluid phase. It simply restricts the solidus lowering action of water to the range below the parameterized solubility of water in the silicate melt.

4.3. Free Parameters and Missing Constraints

[35] Table 2 shows the large number of parameters in this model. This multitude of parameters exists because of a choice in the formulation of the model: each aspect of peridotite melting was parameterized separately resulting in separate "modules," each with a fairly transparent physical meaning. These modules combine to form the melting model but retain their autonomy; each

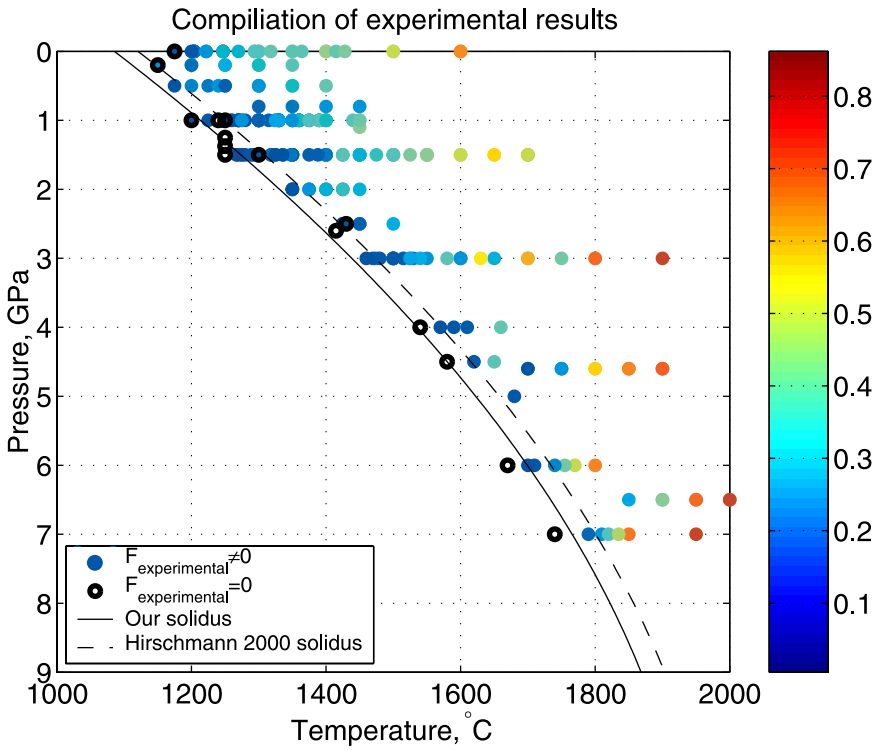

Figure 7. A plot of experimentally determined degree of melting as a function of pressure and temperature. The chosen solidus has an A_1 35°C below that of *Hirschmann* [2000] to better fit the low melt fraction experiments but uses the same A_2 and A_3 that he reported. The 29 experiments within 10°C of the Hirschmann solidus have an average degree of melting of 10 wt%. Of the 29, only 5 have no melting. This is due in part to our inclusion of experiments with more fertile source compositions (e.g., PHN-1611 and MPY) in the database.

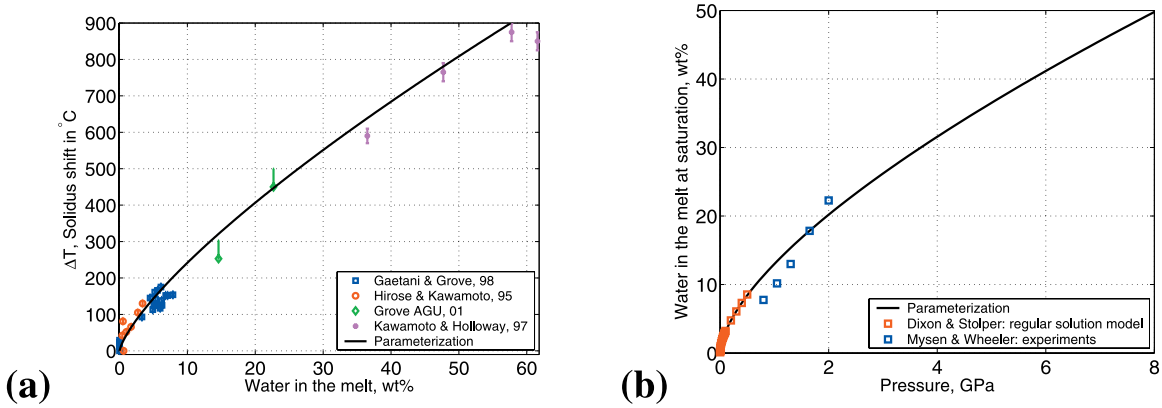

Figure 8. (a) The calibration of $\Delta T(X_{H_2O})$ for the parameters K and γ from equation 16. Data is derived from the experiments of *Hirose and Kawamoto* [1995], *Kawamoto and Holloway* [1997], *Gaetani and Grove* [1998], and *Grove* [2001]. Result is given in Table 2. (b) The saturation water content in wt% of the melt as a function of pressure from equation 17. Points are from *Dixon et al.* [1995], who report a regular solution model for basalt up to 0.5 GPa based on their and other experiments, and *Mysen and Wheeler* [2000], who report the saturation water content for three haploandesitic compositions (shown are results from the aluminum free composition that is 79% SiO_2).

can be analyzed independently against existing or future data and theory. While certain modules are well constrained by existing data, others are poorly constrained at the present. Their values are determined as described above, until more data become available.

[36] The anhydrous liquidii parameters, B_n and C_n, are not well constrained by currently available data. They are essentially fit parameters as described above. The reason for introducing three unconstrained parameters here instead of just one is that they provide greater flexibility to fit experimental data at moderate to high melt fraction, and they are consistent with other parts of the model.

[37] Furthermore, there are sets of model parameters that can trade off to achieve a similar fit to data and constraints. For example, there is a trade-off between a higher curvature of the cpx-in isobaric melting function (β_1) and a lower mantle solidus temperature.

[38] At high pressures, measures of the water saturated solidus constrain $\Delta T(X^{sat}_{H_2O})$; however, the saturation water content at these pressures is unknown. We extrapolate the water saturation curve from low pressures and calibrate the solidus lowering curve to fit the experimentally determined water saturated solidus (see Figures 8a and 8b). A different extrapolation of $X^{sat}_{H_2O}(P)$ would lead to a different $\Delta T(X_{H_2O})$ that would satisfy the same constraint. This ambiguity represents a weakness in the parameterization, especially if it is applied for conditions of high water content and pressures above 2 GPa. This problem could be resolved by direct measurements of water solubility in basaltic melts at high pressure.

[39] Experiments at high pressures indicate that the water-silicate melt solvus may close at about 4 GPa [*Bureau and Keppler*, 1999]. If this is the case, it is incorrect to speak of a water-saturated solidus as there is no saturation point. We extend our parameterization above 4 GPa however, assuming that the parameterized saturation at high pressure is sufficiently high to effectively mimic the possible lack of a saturation point under naturally occurring water contents.

5. Comparison With Other Models

[40] The parameterization of melting described here utilizes current theoretical and experimental results. Older parameterizations exist, however, and have proven useful so it is worth comparing the different parameterizations to each other and to the data. Figures 9 and 10 compare several parameterizations of hydrous and anhydrous melting. This comparison demonstrates that at moderate pressures the parameterizations agree to first order. There are, however, systematic differences at very low and very high degrees of melting. The increasing isobaric productivity above the solidus that is evident in pMELTS calculations and imposed on our parameterization is not present for other anhydrous parameterizations. With the addition of water, however, all of the isobaric melting functions show similar shape for low melt fractions (although the degree of melting can vary significantly between parameterizations). While we have not explored this effect in detail, it suggests that another approach to reconcile all of these models is to assume a linear function of T' for dry melting while employing addition of terms that include the solidus lowering effects of fertility due to fluxing elements such as water or alkalis.

[41] A quantitative measure of the success of a dry melting parameterization is how much of the variance in experiments that it can explain. The parameterizations are applied to each entry in the database using the experimental pressure, temperature (and modal cpx, for our model) to predict a degree of melting. The difference between the experimental and the predicted degree of melting is the residual. The variance reduction is then defined as the percentage of the total variance of experimentally determined F explained by a given parameterization. The variance reduction properties of each of the parameterizations are shown in Table 3. Note that the *Langmuir et al.* [1992] model was not designed for pressures greater than 4 GPa and more than 40% melting.

[42] Clearly a parameterization cannot reduce the variance beyond the experimental uncertainty. Figure 6a shows that under nominally identical conditions ($P \approx 1$ GPa) there is about a 4 wt%

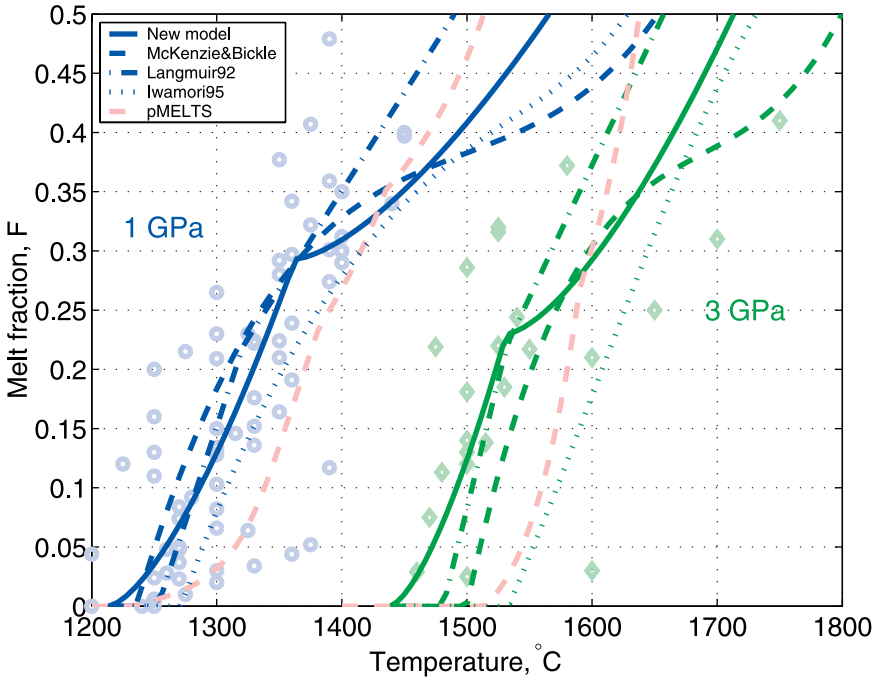

Figure 9. A comparison of the results of several parameterizations of dry melting and pMELTS calculations at 1 (in blue) and 3 (in green) GPa. The parameterizations are described by *Langmuir et al.* [1992], *McKenzie and Bickle* [1988], and *Iwamori et al.* [1995]. pMELTS is described by *Ghiorso et al.* [2002]. A commonly used parameterization by *Kinzler and Grove* [1992] is not considered because it requires the input of chemical information.

standard deviation in melt fraction. At higher pressures this deviation is likely to be greater.

6. Testing and Validation

[43] The intended application for this melting parameterization is the simulation of magma genesis in subduction zones that consider water release from the slab, fluid and solid flow, time dependent reactive melting and chemical transport. Here we concern ourselves with testing and validation of the parameterization by considering two highly simplified examples of magma genesis.

6.1. Adiabatic Upwelling Beneath Mid-Ocean Ridges

[44] A useful test of the melting model is to calculate the melt production of columns of adia-

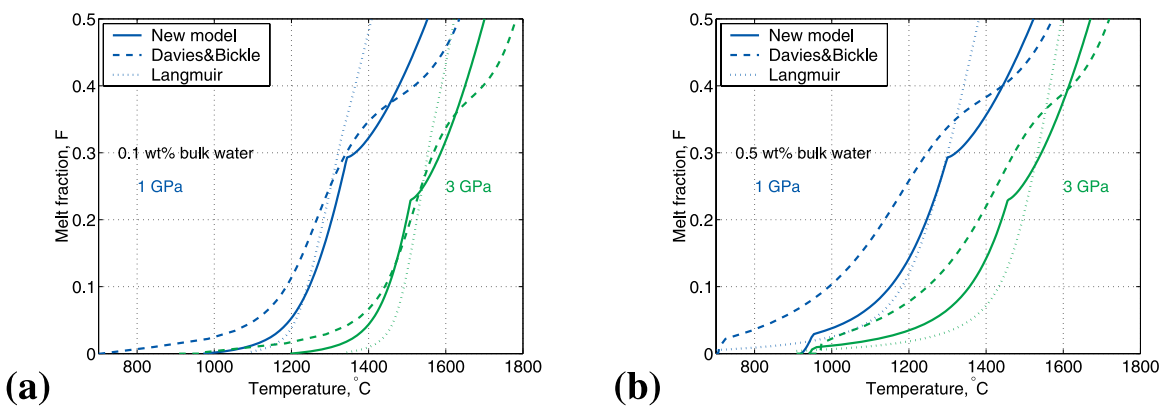

Figure 10. A comparison of parameterizations of mantle melting in the presence of water at 1 and 3 GPa. *Asimow and Langmuir* [2003] use a hydrous extension of the anhydrous parameterization described by *Langmuir et al.* [1992]. *Davies and Bickle* [1991] extends the *McKenzie and Bickle* [1988] parameterization to handle wet melting. (a) For bulk water content of 0.1 wt%. (b) For bulk water content of 0.5 wt%.

Table 3. Summary of Variance Reduction

Parameterization	% Reduction[a]	% Std. Dev. of Residual[a]
New model	85.0	9.1
Langmuir	72.1	13.9
McKenzie & Bickle	74.7	11.0
Iwamori95	74.5	11.2

[a] Using data from anhydrous experiments below 4 GPa and below 40% melting. The use of the entire data set yields lower variance reduction for all parameterizations.

batically upwelling mantle. In this model, melt and solid upwell at the same velocity and do not separate. The melts from each vertical increment of the column may be "pooled" for a simple approximation to a mid-ocean ridge basalt [*Klein and Langmuir*, 1987]. A simplified version of the productivity function for pressure release melting at constant entropy is [*McKenzie*, 1984]

$$\left.\frac{dF}{dP}\right|_S = \frac{-\frac{c_p}{T}\frac{\partial T}{\partial P}\big|_F + F\frac{\alpha_f}{\rho_f} + (1-F)\frac{\alpha_f}{\rho_f}}{\Delta S + \frac{c_p}{T}\frac{\partial T}{\partial F}\big|_P}. \tag{20}$$

Asimow et al. [1997] pointed out that this equation does not account for variation in partial specific entropies of the various phases as a function of *F. Hirschmann et al.* [1999] demonstrated that just above the solidus, when incompatible elements are strongly concentrated in the melt, the effect of partial specific entropy variations may be significant. That said, we employ equation (20) here because we have no way to estimate the partial specific entropies of the solid and fluid phases. For $F < F_{cpx-out}$, the derivatives required for equation (20) are

$$\left.\frac{dT}{dF}\right|_P = \beta_1^{-1} F^{\frac{(1-\beta_1)}{\beta_1}}\left(T^{lherz}_{liquidus} - T_{solidus}\right), \tag{21}$$

$$\left.\frac{dT}{dP}\right|_F = F\beta\left(\frac{\partial T^{lherz}_{liquidus}}{\partial P} - \frac{\partial T_{solidus}}{\partial P}\right) + \frac{\partial T_{solidus}}{\partial P}. \tag{22}$$

For the case where $F > F_{cpx-out}$ similar equations follow directly from equation (8). Equation (20) is numerically integrated using a fourth order Runga-Kutta scheme [*Press et al.*, 1992] from a given pressure and temperature at depth (where $F = 0$) to the surface. The *P-T* paths associated with these melting trajectories are shown in Figure 11b. The *P-T* path of the adiabat is calculated by integrating

$$\left.\frac{dT}{dP}\right|_S = T\left(\frac{F\frac{\alpha_f}{\rho_f} + (1-F)\frac{\alpha_s}{\rho_s} - \Delta S\frac{dF}{dP}\big|_S}{c_P}\right) \tag{23}$$

simultaneously with equation (20). Below the solidus at 1500 K this amounts to about 18 K/GPa.

[45] We calculated adiabatic upwelling columns for 4 values of bulk water content from anhydrous to 200 wt ppm. *Hirth and Kohlstedt* [1996] estimated from the literature that the ambient water content in the mantle is about 125 ± 75 wt ppm. By assuming a potential temperature for the mantle of about 1350°C and a standard activity model for water in silicate melts, they predicted that melting should begin under ridges at about 115 km depth, well within the garnet stability field. Our calculations agree quite well with these estimates, as shown in Figure 11.

[46] Figures 11a and 11b show 12 separate calculations, four bulk water contents at three different mantle potential temperatures. The results agree with the widely held view that water extends the depth interval of melting significantly, putting a larger portion of the total melt generation at higher pressures and increasing the average pressure of melting [*Asimow and Langmuir*, 2003]. In Figure 11c we quantify this effect by plotting the pressure interval over which the first one percent of melting occurs.

6.2. Arc Melting

[47] As a first step toward applying this melting parameterization to subduction zone magma genesis simulations, we calculate a two dimensional melting field on an arc thermal structure with a specified mantle flow field. We apply a constant bulk water concentration evenly over a triangular region of the wedge. The thermal structure is determined by solving a time dependent advection-diffusion equation of energy conservation without melting (we use a Semi-Lagrangian Crank-Nicholson algorithm, see R. Katz, and M. Spiegelman, A semi-Lagrangian Crank-Nicholson algorithm for the numerical solution of advection-diffusion problems, manuscript submitted to *SIAM Journal on Scientific Computing*,

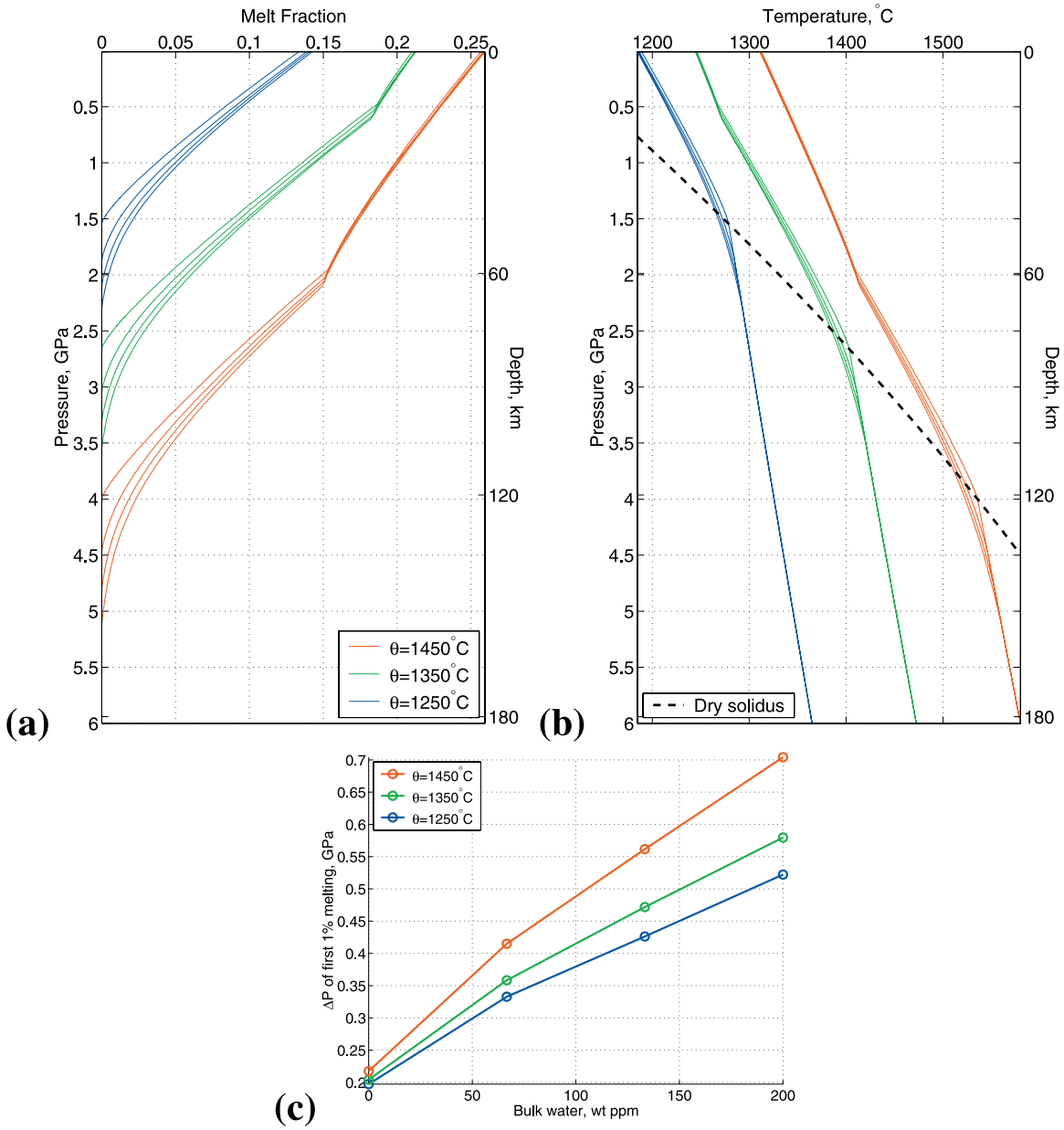

Figure 11. Results of the numerical integration of equations 20 and 23 for a mantle with bulk water ranging from 0 to 200 wt ppm and modal cpx of 10 wt%. Values of all melting model parameters are as given in Table 2. Some of the curves show a kink due to cpx-out. (a) $F(P)$. (b) $T(P)$. (c) A quantification of the water induced low-F tails on adiabats. The pressure interval over which the first one percent of melting occurs is plotted as a function of bulk water in the system and potential temperature.

2003). The thermal calculation is run to steady state and the resulting temperature field is used as an input to the melting calculation. Enthalpy is conserved at each grid point in this calculation according to the equation

$$c_P T_i = (c_P + F\Delta S)T_f. \tag{24}$$

Here, T_i is the temperature before melting and T_f the final temperature after melting. T_f must be consistent with the final degree of melting, F, according to the melt parameterization. Modal cpx is taken as 17 wt%. Results of an example calculation are shown in Figure 12. We explore this model further in Langmuir et al. (manuscript

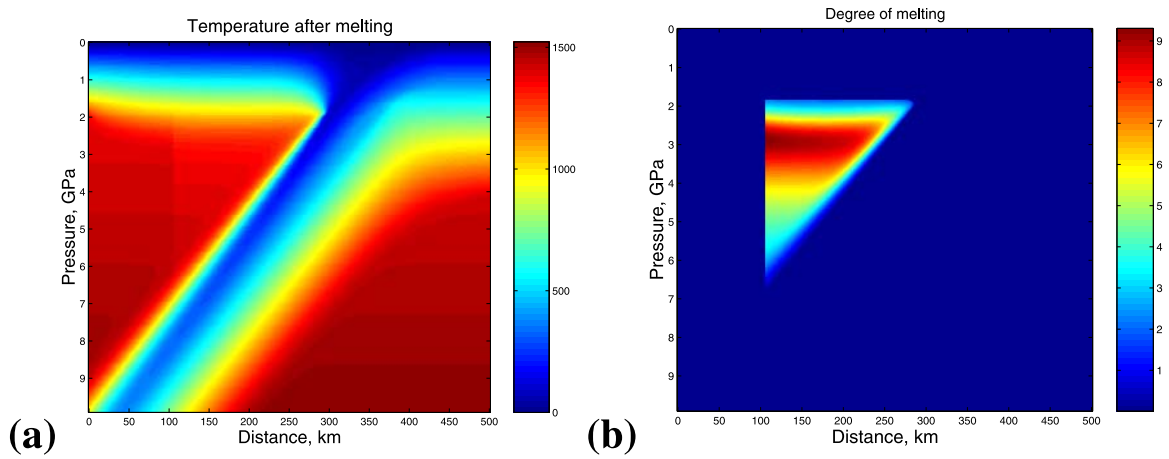

Figure 12. A representative example of a two dimensional static arc melting calculation. Bulk water of 0.5 wt% is applied only over the corner of the wedge shown in (b). The potential temperature of the mantle is taken to be 1350°C. (a) Temperature of equilibration. (b) Equilibrium degree of melting in percent melt by mass. Maximum is 9.3%.

in preparation, 2003) to understand how subduction parameters such as convergence rate and slab dip will affect the degree of melting in the wedge and compare it to Na variations observed in arc lavas.

7. Summary

[48] We have presented a new parameterization of anhydrous and hydrous melting of mantle peridotite that takes into account the pressure, temperature, water content and modal cpx of a melting system to calculate the equilibrium degree of melting. Our parameterization includes many of the important features of hydrous melting of peridotite observed in experiments and predicted by theory. It remains mathematically simple, efficient to compute and flexible to modification as experiments and theory on peridotite melting evolve.

[49] A comparison of isobars shows that all anhydrous parameterizations lie within the experimental variance at moderate pressure. All succeed to a similar degree in fitting the data. Furthermore, all of the parameterizations demonstrate concave upward low-F tails under hydrous conditions. An important difference between the models is their near-solidus behavior under anhydrous conditions.

[50] The first preliminary test of the model, an adiabatic melting calculation, demonstrates that its predictions agree quantitatively with observations and theory [*Hirth and Kohlstedt*, 1996]. An increasing pressure interval for the first 1% melting is consistent with expectations and has important implications for trace element partitioning. Application of the parameterization to a subduction zone thermal calculation gives reasonable results and will be coupled with full fluid and solid flow and geochemical transport in future work.

[51] This parameterization is, of course, a simplification of the natural system that it aims to represent. For example, mineral composition, especially enrichment in easily fusible elements, plays an important role in determining the solidus and the shape of the melting function [*Pickering-Witter and Johnston*, 2000; *Schwab and Johnston*, 2001]. This compositional variability is not captured by our parameterization.

[52] To account for greater variability in the system would require a more complicated model. Given current uncertainties in experimental and theoretical constraints on mantle melting, as well as the need to maintain computational efficiency, we feel that this parameterization contains an appropriate level of detail. It strikes a balance between efficiency and accuracy and delivers output that will be useful in tectonic scale models of magma genesis in subduction zones.

Notation

F	melt fraction
T	temperature, °C
P	pressure, GPa
M_{cpx}	modal cpx by mass
X_{H_2O}	mass fraction water in the liquid phase
$X_{H_2O}^{bulk}$	bulk mass fraction water
$X_{H_2O}^{sat}$	mass fraction water to saturate the silicate liquid
A_n	constants that determine $T_{solidus}$
B_n	constants that determine $T_{liquidus}^{lherz}$
C_n	constants that determine $T_{liquidus}$
β_n	exponents of the melting function
r_n	constants that determine R_{cpx}, the melting reaction coefficient of cpx
K, γ	constant and exponent that determine $\Delta T X_{H_2O}$
D_{H_2O}	bulk distribution coefficient of water between solid peridotite and melt
χ_n, λ	constants and exponent that determine $X_{H_2O}^{sat}(P)$
c_P	specific heat at constant pressure
α_s, α_f	thermal expansivity of the solid and liquid
ρ_s, ρ_f	density of the solid and liquid
ΔS	entropy difference between solid and liquid

Acknowledgments

[53] RK would like to thank P. Asimow for help with MELTS and K_d calculations, T. Plank, K. Kelley, D. Walker, G. Hirth and T. Ruedas for discussions and suggestions. Reviews by M. Hirschmann, G. Gaetani, T. Grove and P. Kelemen were extremely useful.

References

Asimow, P., Modeling hydrous melt production and fractionation at mid-ocean ridges: Application to the Azores region, *J. Conf. Abstr.*, 5, 2000.

Asimow, P., and C. Langmuir, The importance of water to oceanic mantle melting regimes, *Nature*, *421*, 815–820, 2003.

Asimow, P., and E. Stolper, Steady-state mantle-melt interactions in one dimension: I. Equilibrium transport and melt focusing, *J. Petrol.*, *40*, 475–494, 1999.

Asimow, P., M. Hirschmann, and E. Stolper, An analysis of variations in sentropic melt productivity, *Philos. Trans. R. Soc. London Ser. A*, *355*, 255–281, 1997.

Baker, M., and E. Stolper, Determining the composition of high-pressure mantle melts using diamond aggregates, *Geochim. Cosmochim. Acta*, *58*, 2811–2827, 1994.

Baker, M., M. Hirschmann, M. Ghiorso, and E. Stolper, Compositions of near-solidus peridotite melts from experiments and thermodynamic calculations, *Nature*, *375*, 308–311, 1995.

Bureau, H., and H. Keppler, Complete miscibility between silicate melts and hydrous fluids in the upper mantle: Experimental evidence and geochemical implications, *Earth Plan. Sci. Lett.*, *165*, 187–196, 1999.

Burnham, W., The importance of volatile constituents, in *The Evolution of Igneous Rocks: Fiftieth Anniversary Perspectives*, chap. 16, pp. 439–482, Princeton Univ. Press, Princeton, N. J., 1979.

Davies, J., and M. Bickle, A physical model for the volume and composition of melt produced by hydrous fluxing above subduction zones, *Philos. Trans. R. Soc. London Ser. A*, *335*, 355–364, 1991.

Dixon, J., E. Stolper, and J. Holloway, An experimental study of water and carbon dioxide solubilities in mid ocean ridge basaltic liquids: I. Calibration and solubility models, *J. Petrol.*, *36*, 1607–1631, 1995.

Falloon, T., D. Green, L. Danyushevsky, and U. Faul, Peridotite melting at 1.0 and 1.5 GPa: An experimental evaluation of techniques using diamond aggregates and mineral mixes for determination of near-solidus melts, *J. Petrol.*, *40*, 1343–1375, 1999.

Gaetani, G., and T. Grove, The influence of water on melting of mantle peridotite, *Contrib. Mineral. Petrol.*, *131*, 323–346, 1998.

Ghiorso, M., Algorithms for the estimation of phase-stability in heterogeneous thermodynamic systems, *Geochim. Cosmochim. Acta*, *58*, 5489–5501, 1994.

Ghiorso, M., and R. Sack, Chemical mass transfer in magmatic processes. IV. A revised and internally consistent thermodynamic model for the interpolation and extrapolation of liquid-solid equilibria in magmatic systems at elevated temperatures and pressures, *Contrib. Mineral. Petrol.*, *119*, 197–212, 1995.

Ghiorso, M. S., M. M. Hirschmann, P. W. Reiners, and V. C. Kress, III, The pMELTS: A revision of MELTS for improved calculation of phase relations and major element partitioning related to partial melting of the mantle to 3 GPa, *Geochem. Geophys. Geosyst.*, *3*(5), 1030, doi:10.1029/2002GC000217, 2002.

Grove, T., Vapor-saturated melting of fertile peridotite revisited: A new experimental approach and re-evaluation of the hydrous peridotite solidus,, *Eos Trans. AGU*, *82*(47), Fall Meet. Suppl., Abstract T31F-05, 2001.

Hirose, K., Melting experiments on lherzolite KLB-1 under hydrous conditions and generation of high-magnesian andesitic melts, *Geology*, *25*, 42–44, 1997.

Hirose, K., and T. Kawamoto, Hydrous partial melting of lherzolite at 1 Gpa: The effect of H2O on the genesis of basaltic magmas, *Earth Planet. Sci. Lett.*, *133*, 463–473, 1995.

Hirose, K., and I. Kushiro, Partial melting of dry peridotites at high-pressures-determination of compositions of melts

segregated from peridotite using aggregates of diamond, *Earth Planet. Sci. Lett.*, *114*, 477–489, 1993.

Hirschmann, M., Mantle solidus: Experimental constraints and the effect of peridotite composition, *Geochem. Geophys. Geosyst.*, *1*, Paper number 2000GC000070, 2000.

Hirschmann, M., P. Asimow, M. Ghiorso, and E. Stolper, Calculation of peridotite partial melting from thermodynamic models of minerals and melts: III. Controls on isobaric melt production and the effect of water on melt production, *J. Petrol.*, *40*, 831–851, 1999.

Hirth, G., and D. Kohlstedt, Water in the oceanic upper mantle: implications for rheology, melt extraction and the evolution of the lithosphere, *Earth Planet. Sci. Lett.*, *144*, 93–108, 1996.

Ihinger, P., Y. Zhang, and E. Stolper, The speciation of dissolved water in rhyolitic melt, *Geochim. Cosmochim. Acta*, *63*, 3567–3578, 1999.

Iwamori, H., Compression melting in subduction zones, *Terr. Nova*, *9*, 9–13, 1997.

Iwamori, H., D. McKenzie, and E. Takahashi, Melt generation by isentropic mantle upwelling, *Earth Planet. Sci. Lett.*, *134*, 253–266, 1995.

Jaques, A., and D. Green, Anhydrous melting of peridotite at 0–15 kb pressure and the genesis of tholeiitic basalts, *Contrib. Mineral. Petrol.*, *73*, 287–310, 1980.

Jha, K., E. Parmentier, and J. Phipps Morgan, The role of mantle-depletion and melt-retention buoyancy in spreading-center segmentation, *Earth Planet. Sci. Lett.*, *125*, 221–234, 1994.

Kawamoto, T., and J. Holloway, Melting temperature and partial melt chemistry of H_2O-saturated mantle peridotite to 11 gigapascals, *Science*, *276*, 240–243, 1997.

Kelemen, P. B., H. J. Dick, and J. E. Quick, Formation of harzburgite by pervasive melt rock reaction in the upper mantle, *Nature*, *358*, 635–641, 1992.

Kinzler, R., Melting of mantle peridotite at pressures approaching the spinel to garnet transition: Application to mid-ocean ridge basalt petrogenesis, *J. Geophys. Res.*, *102*, 853–874, 1997.

Kinzler, R., and T. Grove, Primary magmas of midocean ridge basalts: 1. Experiments and methods, *J. Geophys. Res.*, *97*, 6885–6906, 1992.

Klein, E. M., and C. H. Langmuir, Global correlations of ocean ridge basalt chemistry with axial depth and crustal thickness, *J. Geophys. Res.*, *92*, 8089–8115, 1987.

Kogiso, T., K. Hirose, and E. Takahashi, Melting experiments on homogeneous mixtures of peridotite and basalt: Application to the genesis of ocean island basalts, *Earth Planet. Sci. Lett.*, *162*, 45–61, 1998.

Kushiro, I., Partial melting of a fertile mantle peridotite at high pressures: An experimental study using aggregates of diamond, in *Earth Processes: Reading the Isotopic Code*, *Geophys. Monogr. Ser.*, vol. 95, edited by A. Basu and S. Hart, pp. 109–122, AGU, Washington, D.C., 1996.

Langmuir, C., and G. Hanson, Calculating mineral-melt equilibria with stoichiometry, mass balance, and single-component distributions, in *Thermodynamics of Minerals and Melts*, edited by R. Newton, A. Navrotsky, and B. Wood, *Adv. Phys. Geochem.*, *1*, 247–272, 1981.

Langmuir, C., E. Klein, and T. Plank, Petrological systematics of mid-oceanic ridge basalts: Constraints on melt generation beneath ocean ridges, in *Mantle Flow and Melt Generation at Mid-Ocean Ridges*, *Geophys. Monogr. Ser.*, vol. 71, edited by J. Phipps Morgan, D. Blackman, and J. Sinton, pp. 183–280, AGU, Washington, D.C., 1992.

Longhi, J., Some phase equilibrium systematics of lherzolite melting: I, *Geochem. Geophys. Geosyst.*, *3*(3), 1020, doi:10.1029/2002GC000204, 2002.

McKenzie, D., The generation and compaction of partially molten rock, *J. Petrol.*, *25*, 713–765, 1984.

McKenzie, D., and M. Bickle, The volume and composition of melt generated by extension of the lithosphere, *J. Petrol.*, *29*, 625–679, 1988.

Michael, P., Regionally distinctive sources of depeleted MORB: Evidence from trace elements and H_2O, *Earth Planet. Sci. Lett.*, *131*, 301–320, 1995.

Mosenfelder, J., N. Deligne, A. P.D., and G. Rossman, Incorporation of oh in olivine at high pressure: New experimental results, in, *AGU Eos Trans.*, *83*(47), Fall Meet. Suppl., Abstract T22C-07, 2002.

Mysen, B., and K. Wheeler, Solubility behavior of water in haploandesitic melts at high pressure and high temperature, *Am. Mineral.*, *85*, 1128–1142, 2000.

Pickering-Witter, J., and A. Johnston, The effects of variable bulk composition on the melting systematics of fertile peridotitic assemblages, *Contrib. Mineral. Petrol.*, *140*, 190–211, 2000.

Press, W., S. Teukolsky, W. Vetterling, and B. Flannery, Numerical Recipes in *FORTRAN: The Art of Scientific Computing*, 2nd ed., Cambridge Univ. Press, New York, 1992.

Robinson, J., B. Wood, and J. Blundy, The beginning of melting of fertile and depleted peridotite at 1.5 GPa, *Earth Planet. Sci. Lett.*, *155*, 97–111, 1998.

Schmidt, M. W., and S. Poli, Experimentally based water budgets for dehydrating slabs and consequences for arc magma generation, *Earth Planet. Sci. Lett.*, *163*, 361–379, 1998.

Schwab, B., and A. Johnston, Melting systematics of modally variable, compositionally intermediate peridotites and the effects of mineral fertility, *J. Petrol.*, *42*, 1789–1811, 2001.

Spiegelman, M., Flow in deformable porous media: Part 1. Simple analysis, *J. Fluid Mech.*, *247*, 17–38, 1993.

Stolper, E., The temperature dependence of the speciation of water in rhyolitic melts and glasses, *Am. Mineral.*, *74*, 1247–1257, 1989.

Takahashi, E., Melting of a dry peridotite KLB-1 up to 14 GPa-Implications on the origin of peridotitic upper mantle, *J. Geophys. Res.*, *91*, 9367–9382, 1986.

Takahashi, E., T. Shimazaki, Y. Tsuzaki, and H. Yoshida, Melting study of a peridotite KLB-1 to 6.5 GPa, and the origin of basaltic magmas, *Philos. Trans. R. Soc. London Ser. A*, *342*, 105–120, 1993.

Tirone, M., and J. Ganguly, Thermodynamic control on thermo-fluid dynamic mantle flow model, paper presented at Goldschmidt Conference, Eur. Assoc. of Geochem., Davos, Switzerland, 2002.

Walter, M., Melting of garnet peridotite and the origin of komatiite and depleted lithosphere, *J. Petrol.*, *39*, 29–60, 1998.

Walter, M., T. Sisson, and D. Presnall, A mass proportion method for calculating melting reactions and application to melting of model upper mantle lherzolite, *Earth Planet. Sci. Lett.*, *135*, 77–90, 1995.

Weaver, J., and C. Langmuir, Calculation of phase equilibrium in mineral-melt systems, *Comput. Geosci.*, *16*, 1–19, 1990.

Withers, A., Y. Zhang, and H. Behrens, Reconciliation of experimental results on H_2O speciation in rhyolitic glass using in-situ and quenching techniques, *Earth Planet. Sci. Lett.*, *173*, 343–349, 1999.